



HAL
open science

Strong impacts of biomass burning, nitrogen fertilization, and fine particles on gas-phase hydrogen peroxide (H₂O₂)

Can Ye, Chaoyang Xue, Pengfei Liu, Chenglong Zhang, Zhuobiao Ma, Yuanyuan Zhang, Chengtang Liu, Junfeng Liu, Keding Lu, Yujing Mu

► To cite this version:

Can Ye, Chaoyang Xue, Pengfei Liu, Chenglong Zhang, Zhuobiao Ma, et al.. Strong impacts of biomass burning, nitrogen fertilization, and fine particles on gas-phase hydrogen peroxide (H₂O₂). *Science of the Total Environment*, 2022, 843, pp.156997. 10.1016/j.scitotenv.2022.156997. insu-04046942

HAL Id: insu-04046942

<https://insu.hal.science/insu-04046942v1>

Submitted on 27 Sep 2024

HAL is a multi-disciplinary open access archive for the deposit and dissemination of scientific research documents, whether they are published or not. The documents may come from teaching and research institutions in France or abroad, or from public or private research centers.

L'archive ouverte pluridisciplinaire **HAL**, est destinée au dépôt et à la diffusion de documents scientifiques de niveau recherche, publiés ou non, émanant des établissements d'enseignement et de recherche français ou étrangers, des laboratoires publics ou privés.



Distributed under a Creative Commons Attribution 4.0 International License

1 Strong Impacts of Biomass Burning, Nitrogen Fertilization, and Fine 2 Particles on Gas-phase Hydrogen Peroxide (H₂O₂)

3 Can Ye^{1,2}, Chaoyang Xue^{3*}, Pengfei Liu^{1,4,5}, Chenglong Zhang^{1,4,5}, Zhuobiao Ma^{1,4,5}, Yuanyuan
4 Zhang^{1,4,5}, Chengtang Liu^{1,4,5}, Junfeng Liu^{1,4,5}, Keding Lu², Yujing Mu^{1,4,5*}.

5 ¹Research Centre for Eco-Environmental Sciences, Chinese Academy of Sciences, Beijing 100085, China

6 ²State Key Joint Laboratory of Environmental Simulation and Pollution Control, College of Environmental Sciences and
7 Engineering, Peking University, Beijing 100871, China.

8 ³Laboratoire de Physique et Chimie de l'Environnement et de l'Espace (LPC2E), CNRS – Université Orléans – CNES,
9 45071 Orléans Cedex 2, France

10 ⁴Centre for Excellence in Regional Atmospheric Environment, Institute of Urban Environment, Chinese Academy of
11 Sciences, Xiamen 361021, China

12 ⁵University of Chinese Academy of Sciences, Beijing 100049, China

13

14 *Correspondence to:* Chaoyang Xue (chaoyang.xue@cnrs-orleans.fr), Yujing Mu (yjmu@rcees.ac.cn)

15 **Abstract.** Gas-phase hydrogen peroxide (H₂O₂) plays an important role in atmospheric chemistry as an indicator of the
16 atmospheric oxidizing capacity. It is also a vital oxidant of sulfur dioxide (SO₂) in the aqueous phase, resulting in the
17 formation of acid precipitation and sulfate aerosol. However, sources of H₂O₂ are not fully understood especially in
18 polluted areas affected by human activities. In this study, we reported some high H₂O₂ cases observed during one
19 summer and two winter campaigns conducted at a polluted rural site in the North China Plain. Our results showed that
20 agricultural fires led to high H₂O₂ concentrations up to 9 ppb, indicating biomass burning events contributed
21 substantially to primary H₂O₂ emission. In addition, elevated H₂O₂ and O₃ concentrations were measured after

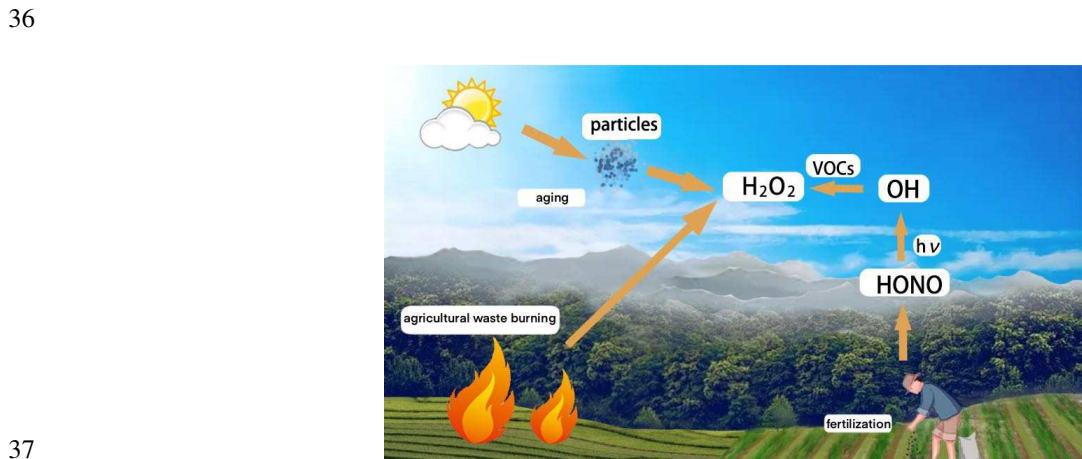
22 fertilization as a consequence of the enhanced atmospheric oxidizing capacity by soil HONO emission. Furthermore,
23 H₂O₂ exhibited unexpectedly high concentration under high NO_x conditions in winter, which are closely related to
24 multiphase reactions in particles involving organic chromophores. Our findings suggest that these special factors
25 (biomass burning, fertilization, and ambient particles), which are not well considered in current models, are significant
26 contributors to H₂O₂ production, thereby affecting the regional atmospheric oxidizing capacity and the global sulfate
27 aerosol formation.

28
29 Key words: H₂O₂, biomass burning, fertilization, particles, organic chromophores

30
31 **Highlights**

- 32 ● Biomass burning events led to high H₂O₂ concentrations up to 9 ppb observed.
- 33 ● H₂O₂ and O₃ were greatly enhanced after fertilization events due to HONO emission by fertilized soil.
- 34 ● Particle-phase reactions involving organic chromophores contributed to H₂O₂ production.

35 **Graphical abstract**

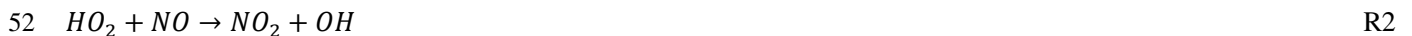


38 1 Introduction

39 Atmospheric hydrogen peroxide (H_2O_2) acts as a temporary reservoir of HO_x ($OH+HO_2$) radicals and hence an
40 indicator of the oxidizing capacity of the atmosphere. Besides, H_2O_2 itself is one of the most important oxidants in the
41 atmosphere and can oxidize SO_2 in clouds, droplets, and deliquesced particles (Penkett et al., 1979; Calvert and
42 Stockwell, 1983), with the formation of sulfate, an important component of fine particulate matter that impacts air
43 quality, climate, and human health (Grantz et al., 2003; Nel, 2005; Fuzzi et al., 2015). Furthermore, H_2O_2/HNO_3 was
44 suggested as a robust indicator to determine whether ozone production is more sensitive to NO_x or VOCs (Sillman,
45 1995; Sillman et al., 1998). Vermeuel et al. (2019) evaluated the sensitivity of O_3 to VOCs and NO_x alongside the
46 Lake Michigan Coastline utilizing the modeled ratio of H_2O_2 and HNO_3 production rates. Results indicated that the O_3
47 production was strongly VOC-limited in the urban areas and became more NO_x -limited as the plume advected North.
48 As O_3 pollution is becoming a big concern with increase of NO_x and VOCs emissions (Tan et al., 2018; Yu et al.,
49 2020), H_2O_2 has drawn more attention in both urban and rural areas.



51 $k_{R1}=1.5\times 10^{-12} \text{ cm}^3 \text{ molecule}^{-1} \text{ s}^{-1}$ at 298 K



53 $k_{R2}=8.9\times 10^{-12} \text{ cm}^3 \text{ molecule}^{-1} \text{ s}^{-1}$ at 298 K

54 Based on the current understanding, H_2O_2 is mainly produced by the self-reaction of two hydroperoxy radicals (HO_2)
55 (R1), which are produced from the oxidation of hydrocarbons by OH radicals or the photolysis of formaldehyde. R1
56 largely depends on ambient NO_x levels. With high NO_x levels, R2 would dominate relative to R1 due to more rapid
57 HO_2 consumption through R2. For example, with typical noontime NO concentration of 1 ppb and HO_2 concentration
58 of $4\times 10^7 \text{ molecules cm}^{-3}$ observed or modelled in the winter NCP (Ma et al., 2019; Slater et al., 2020; Xue et al., 2020),
59 HO_2 loss rate through R2 ($8.4\times 10^6 \text{ molecules cm}^{-3} \text{ s}^{-1}$) is 3 orders of magnitude faster than that of R1 (2.6×10^3
60 $\text{molecules cm}^{-3} \text{ s}^{-1}$). Field measurements also supported that under the condition of NO concentrations exceeding 1

61 ppb, H₂O₂ production through R1 will be substantially suppressed (Walker et al., 2006; He et al., 2010; Watanabe et
62 al., 2018). Besides the H₂O₂ formation channel through R1, ozonolysis of alkenes also contributes to H₂O₂ production,
63 which could proceed without sunlight (Becker et al., 1990; Hua et al., 2008). The main sinks of H₂O₂ include
64 photolysis, dry deposition, reaction with OH radicals, and reaction with SO₂ in the liquid phase. The typical photolysis
65 rate of H₂O₂ daily maximum value is $6.0 \times 10^{-6} \text{ s}^{-1}$ in the northern midlatitude (Stockwell et al., 1997), corresponding to
66 $\tau_{\text{photo}}=46 \text{ h}$ (lifetime against photolysis). As for the reaction of H₂O₂ with OH radicals, the rate constant is 1.7×10^{-12}
67 $\text{cm}^3 \text{ molecule}^{-1} \text{ s}^{-1}$ at 298 K (Atkinson et al., 2004), and the temperature influence on the rate constant is small. $\tau_{\text{H}_2\text{O}_2}$
68 (lifetime with respect to OH reaction) is estimated to be around 32 h if OH concentration is assumed to be 5×10^6
69 molecule cm^{-3} . Assuming the dry deposition velocity of H₂O₂ is about 2 cm s^{-1} (Liang et al., 2013), the lifetime of
70 H₂O₂ with respect to dry deposition is 7 h with a boundary height of 1 km. Therefore, dry deposition loss was a
71 dominant factor influencing the lifetime of H₂O₂ in the atmosphere.

72 H₂O₂ formation does not only depend on NO_x levels, which was discussed earlier but also as a function of many other
73 chemical and physical parameters. First of all, H₂O₂ concentrations are affected by precursors concentrations like
74 VOCs. High VOC to NO_x ratio leads to more HO₂ production, in favor of the production of H₂O₂ (Lee et al., 2008;
75 Crowley et al., 2018). O₃ and HONO, which are important contributors to OH radicals in the lower troposphere, also
76 have crucial effect on H₂O₂ formation under certain atmospheric conditions. For instance, in a clean environment, OH
77 radicals mainly come from O₃ photolysis followed by the reaction of O(¹D) with water vapor. In polluted areas (like
78 urban sites), HONO appeared to be an important source of OH radicals (Elshorbany et al., 2010; Xue et al., 2020). In
79 addition, since H₂O₂ is very soluble with high Henry's law constant of $1.07 \times 10^5 \text{ M atm}^{-1}$ at 298 K (Lee et al., 2000;
80 Reeves and Penkett, 2003), H₂O₂ can be readily consumed via reaction with SO₂ in the atmospheric aqueous phase
81 (Penkett et al., 1979; Hoffmann and Edwards, 1975). Hence, high SO₂ concentrations are usually associated with low
82 H₂O₂ concentrations (Watanabe et al., 2016; Guo et al., 2014). Moreover, solar radiation has a significant impact on
83 H₂O₂ concentrations. Model simulations by Kleinman et al. showed that a 60% decrease in solar radiation intensity
84 could lead to a 65% decrease in H₂O₂ concentrations (Kleinman, 1986), which highlights the important role of solar

85 radiation in the formation of H₂O₂. The absolute humidity is an important factor for H₂O₂ formation as high humidity
86 may lead to an increase in OH radical and hence more H₂O₂ production (Hamilton Jr and Lii, 1977; Fischer et al.,
87 2019). Also, higher temperature promotes the rate of photochemical reactions, resulting in more radical production and
88 hence more H₂O₂ production (Das and Aneja, 1994; Nunnermacker et al., 2008; Zhang et al., 2018). These factors are
89 well understood and all considered in the box model and regional transport models. However, it was reported that
90 H₂O₂ was still underestimated during polluted periods, indicating that some extra factors affecting H₂O₂ concentrations
91 may be neglected (Qin et al., 2018; Ye et al., 2018). Moreover, there is still a gap between modeled and measured
92 sulfate concentrations during haze events, suggesting sulfate formation is not completed in current mechanisms (Wang
93 et al., 2014; Zheng et al., 2015). Hence, it is essential to incorporate all processes related to H₂O₂ formation into
94 regional models for better predictions. However, there is a relatively small body of literature that is concerned with
95 gas-phase H₂O₂ measurements in China (Wang et al., 2016; Qin et al., 2018; Ye et al., 2018; Zhang et al., 2018),
96 especially in the North China Plain (NCP) where it is encountering serious air pollution.

97 In order to more accurately predict H₂O₂ concentrations and evaluate its role in the oxidizing capacity of the
98 atmosphere, a comprehensive investigation of factors controlling gaseous H₂O₂ should be conducted. In this study,
99 H₂O₂ and other relevant pollutants were simultaneously measured at a polluted rural site in the NCP in summertime
100 (31 May to 8 July 2017) and wintertime (1 November to 31 December 2017, 1 to 15 December 2018). Time series of
101 H₂O₂ and related parameters in the three field campaigns were shown in Figure S1. In addition to the factors mentioned
102 above, some special factors were also found to profoundly affect atmospheric H₂O₂ concentrations in our study, which
103 might be overlooked by the current understanding. The following will be some cases observed in our field
104 measurements to reveal these special factors.

105 **2 Experiments**

106 **2.1 Measurement site**

107 The measurements were conducted at a rural site (SRE-CAS, 38.66°N, 115.25°E) located in Wangdu County (Liu et
108 al., 2017; Xue et al., 2020), in Hebei province, which is 150 km southwest of Beijing city in the NCP. This site was
109 surrounded by vast areas of farmlands and impacted by coal combustion in winter and agricultural activities such as
110 biomass burning and fertilization in summer. A high-speed way was located 2 km southwest of the site. There are no
111 industries around the sampling site. All instruments were placed into a container with the sampling inlet about 3.4 m
112 above the ground.

113 **2.2 Measurement methods**

114 A Germany commercial H₂O₂ monitor (AEROLASER AL-2021) based on a wet chemical technique was employed to
115 measure gas-phase H₂O₂. Firstly, soluble peroxides, including H₂O₂ and organic peroxides, were sampled by a
116 stripping coil with a buffered solution. In order to distinguish H₂O₂ and organic peroxides, the stripping solution was
117 divided into two channels. In the first channel, the peroxides in the stripping solution react with p-hydroxyphenyl
118 acetic acid (POPHA) under the catalysis of peroxidase, resulting in the formation of fluorescent dye. After excitation at
119 326 nm, the fluorescence could be detected at 400-420 nm. In the second channel, before peroxides reaction with
120 POPHA, enzyme catalase was added to selectively destroy H₂O₂. Then H₂O₂ was determined as the difference between
121 the two channels. Liquid calibration was performed every two days. The detection limit of the instrument was <50 ppt.
122 Detailed information can be found in our previous study (Ye et al., 2018).

123 HONO was measured by a commercial long path absorption photometer instrument (LOPAP, Model-03, QUMA)
124 (Heland et al., 2001). Briefly, ambient air was sampled by using two same stripping coils connected in series. Because
125 HONO is highly soluble, almost all the ambient HONO was absorbed by the absorption solution in the first stripping
126 coil, while possibly interfering species were sampled in the first as well as the second stripping coil. Thus, the signal

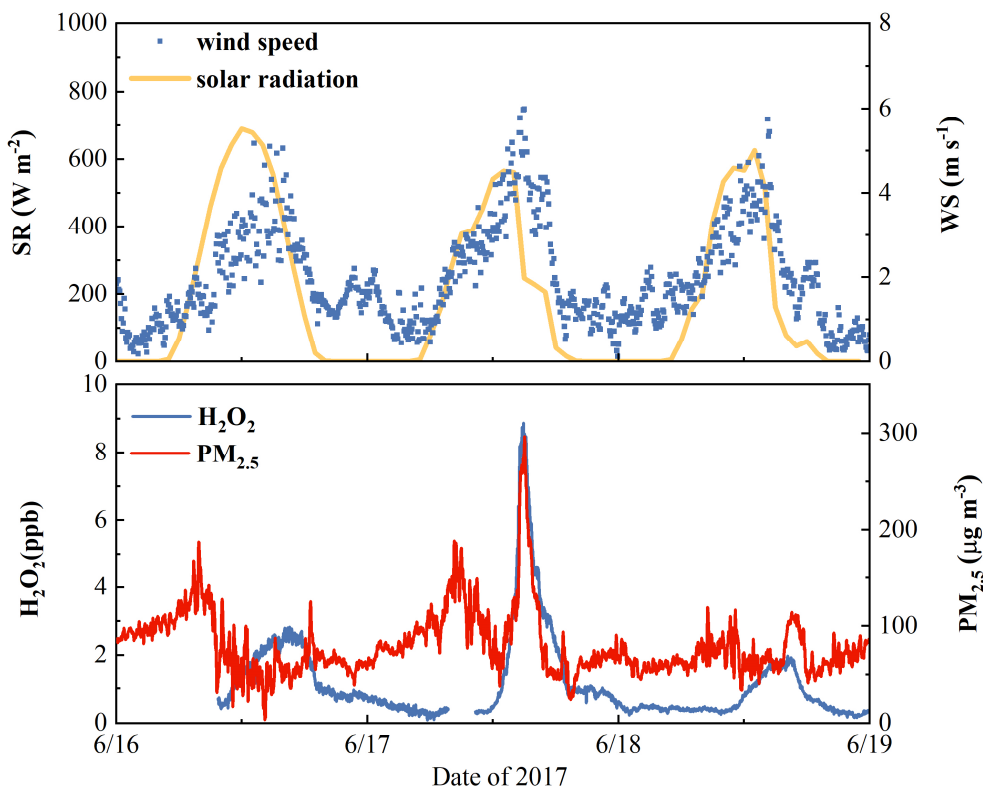
127 difference between the two channels can largely eliminate the possible influence of the interfering species on the
128 HONO measurement. Instrument background was conducted by sampling ultrapure nitrogen twice per day. The
129 instrument has a detection limit of <5 ppt on 5 min average.

130 NO and NO₂ were measured with a chemiluminescence analyzer (Thermo Environmental Instruments (TEI), Model
131 42i) equipped with a photolytic converter. Ozone (O₃) was measured by a commercial UV photometric analyzer (TEI
132 Model 49i). SO₂ was measured by a pulsed fluorescence SO₂ analyzer (Model 43i). The analyzers of NO_x (NO/NO₂),
133 O₃ and SO₂ were regularly calibrated once per week. PM_{2.5} levels were measured by a standard Tapered Element
134 Oscillating Microbalance system (TEOM 1400A, Thermo Scientific). Organic carbon (OC) and elemental carbon (EC)
135 were measured by using an online organic/elemental carbon analyzer (TR20N9, CECEP Talroad Technology Co.,
136 Ltd., China). Meteorological measurements (temperature, pressure, wind speed and direction, relative humidity, and
137 solar radiation) were achieved by a portable weather station (Model WXT520, Vaisala, Finland).

138 **3 Results and discussion**

139 **3.1 Influence of biomass burning events on H₂O₂ chemistry**

140 Figure 1 depicts the time series of H₂O₂, PM_{2.5}, and some meteorological parameters from 16 to 19 June 2017. H₂O₂
141 exhibited a typical diurnal pattern with a maximum in the early afternoon and low concentrations during the night and
142 in the morning. For instance, on 16 June, H₂O₂ reached a maximum value of ~2.5 ppb around 15:00 LST (Local
143 Standard Time). However, at 13:00 LST on the following day, H₂O₂ increased remarkably from ~1 to ~9 ppb in two
144 hours. Notably, PM_{2.5} also increased concurrently with H₂O₂ from ~50 to ~300 μg m⁻³.

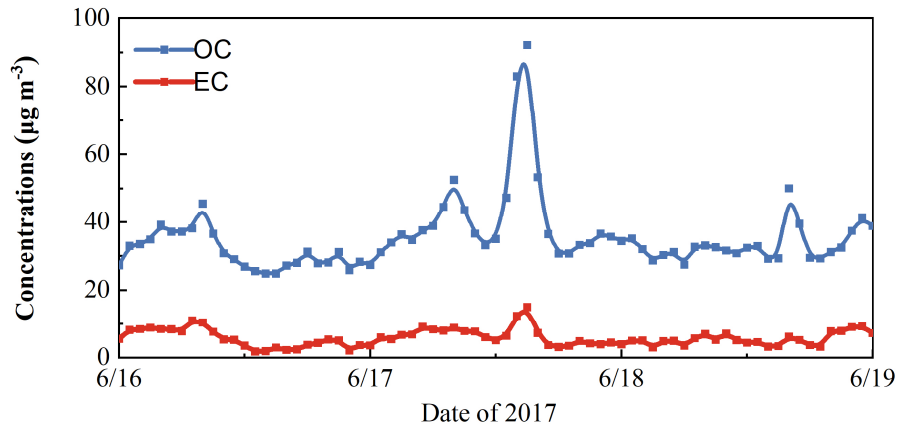


145

146 **Figure 1: Time series of H_2O_2 , $\text{PM}_{2.5}$, solar radiation, and wind speed from 16 to 19 June 2017 in the summer**
 147 **campaign. H_2O_2 and $\text{PM}_{2.5}$ were shown in minute-average data.**

148 The significantly positive correlation between H_2O_2 and $\text{PM}_{2.5}$ from 13:00 to 18:00 during the event ($r^2=0.97$)
 149 indicated the same reason for their increases. However, the wind speed was high during the elevation period ($\sim 4\text{-}6 \text{ m s}^{-1}$),
 150 and there wasn't a significant difference in the solar radiation with regard to other days, indicating photochemical
 151 reactions alone couldn't explain the sharp increase of H_2O_2 in such a short period. Considering the high wind speed
 152 when the high H_2O_2 event was observed, the exceptionally high H_2O_2 might be ascribed to the regional transport of
 153 H_2O_2 from the emission source. In addition, the OC (organic carbon) to EC (elemental carbon) ratio at 15:00 LST
 154 being higher than 5 (Figure 2) suggested a biomass burning event encountered here (Watson et al., 2001). The well-
 155 defined shape and narrow width of the observed H_2O_2 within the plume indicated that the plume had not experienced

156 significant dispersion and mixing since it was emitted, suggesting that the sampling site is not far from the emission
157 source.

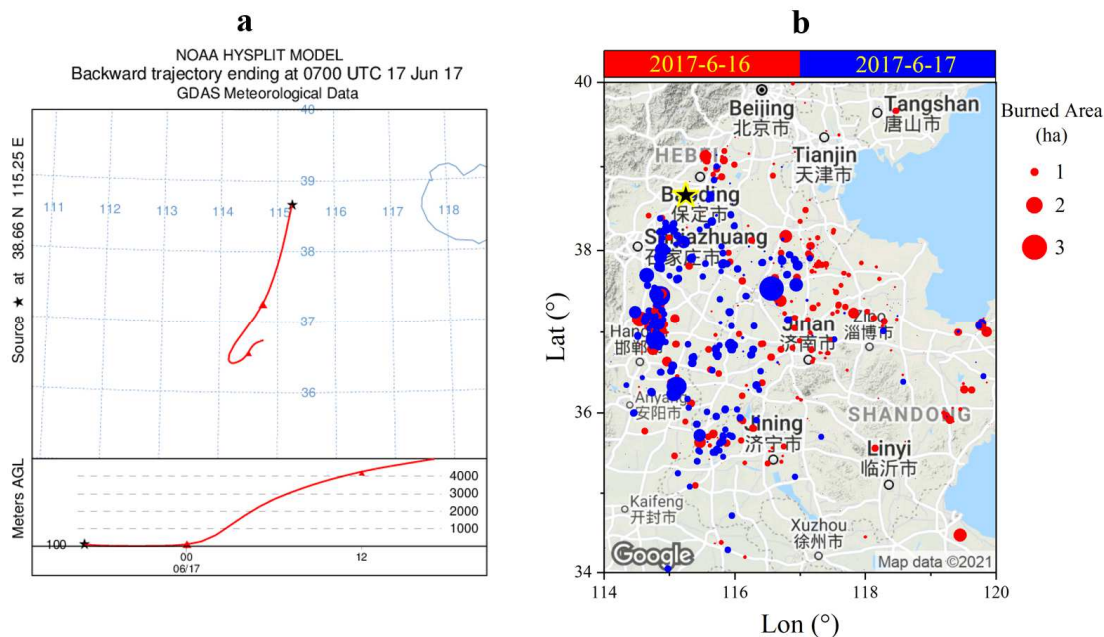


158

159 **Figure 2: Time series of OC and EC from 16 to 19 June 2017 in the summer campaign.**

160 Given the short lifetime of H_2O_2 in the atmosphere (typically less than one day), we calculated 1-day back trajectory
161 with the HYSPLIT model (<https://www.ready.noaa.gov/HYSPLIT.php>, last access: 15 April 2022) and found the
162 sampling site was influenced by the plume coming from the southern areas (Figure 3a). The fire spot data on 16 June
163 and 17 June showed that south areas were filled with dense fire spots (Figure 3b), indicative of large areas of
164 agricultural (wheat straw) fires. Large areas of biomass burning in farmland contributed to the primary H_2O_2 emission,
165 resulting in the high H_2O_2 concentrations measured at the downwind site. Lee et al. (1997) observed H_2O_2
166 concentrations up to 10 ppb and attributed this to the direct production of H_2O_2 within biomass burning plumes. Some
167 studies also found an underestimation of modelled H_2O_2 concentration compared with observations during biomass
168 burning events (Wang et al., 2016; Crowley et al., 2018). H_2O_2 concentrations at our sampling site increased by a
169 factor of ~ 5 (from ~ 2 ppb to ~ 9 ppb), which is larger than the value (1.2-3.6) observed in biomass burning plumes by a
170 recent study (Allen et al., 2022). The difference may be explained by the different photochemical age of the air mass
171 sampled. In addition to primary emission, H_2O_2 concentrations will also increase with the photoaging of the biomass
172 burning plume as a consequence of abundant precursors contributing to secondary H_2O_2 production (Yokelson et al.,
173 2009). Moreover, low NO_x levels at the rural areas are conducive for secondary H_2O_2 production. Unfortunately, we

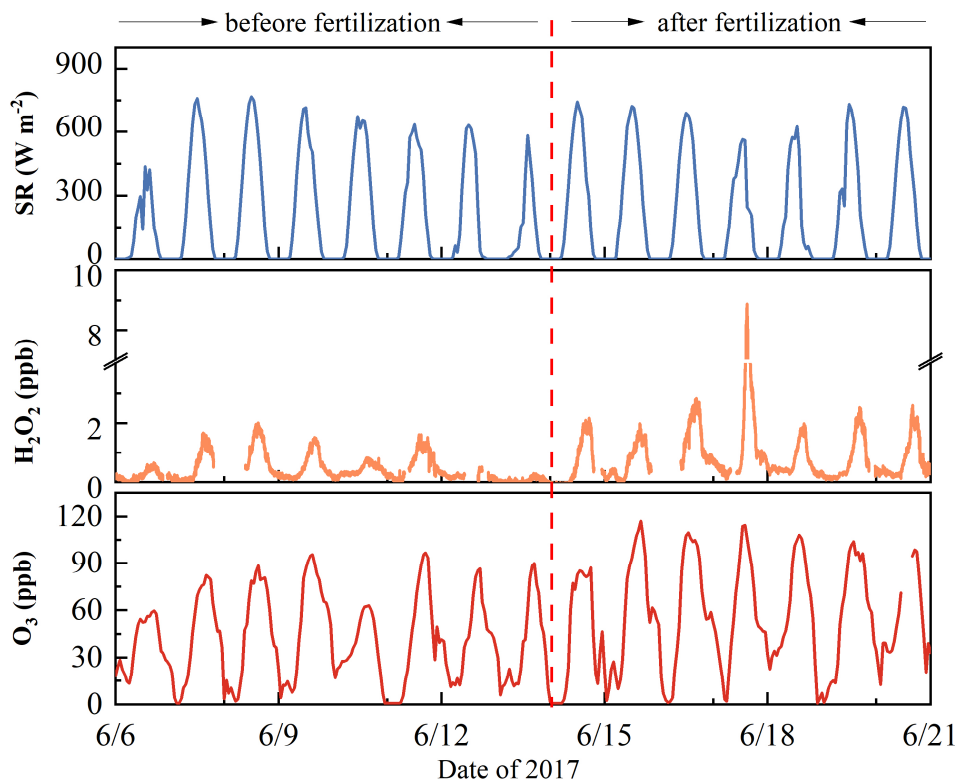
174 are unable to distinguish primary emission from secondary production during the plume transport. Our results provided
 175 direct field evidence that biomass burning events significantly affect H₂O₂ concentrations, despite the polluted plume
 176 was already aged or diluted. The primary and secondary H₂O₂ produced from biomass burning contributes to odd-
 177 hydrogen radicals, thereby affecting the oxidizing capacity of the atmosphere. Given that wildfire is increasing
 178 globally and agricultural fires can be commonly seen during harvesting seasons worldwide (Andreae et al., 2019; Liu
 179 et al., 2015), they are expected to make great contributions to H₂O₂ production. To better evaluate the global
 180 consequence of the biomass burning-related H₂O₂ production, the emission factor and the production mechanism need
 181 to be critically determined.



182
 183 **Figure 3. (a) 24 h-trajectory arriving at SRE-CAS site at 15:00 (UTC+8), 17 July 2017 when the peak H₂O₂**
 184 **occurred. (b) Fire spots map on 16 and 17 June 2017 UTC time obtained from the FINN biomass burning**
 185 **inventory (Wiedinmyer et al., 2011). The sampling site is represented by a black triangle. Map copyright:**
 186 **GoogleMap.**

187 **3.2 Influence of nitrogen fertilization on the H₂O₂ chemistry**

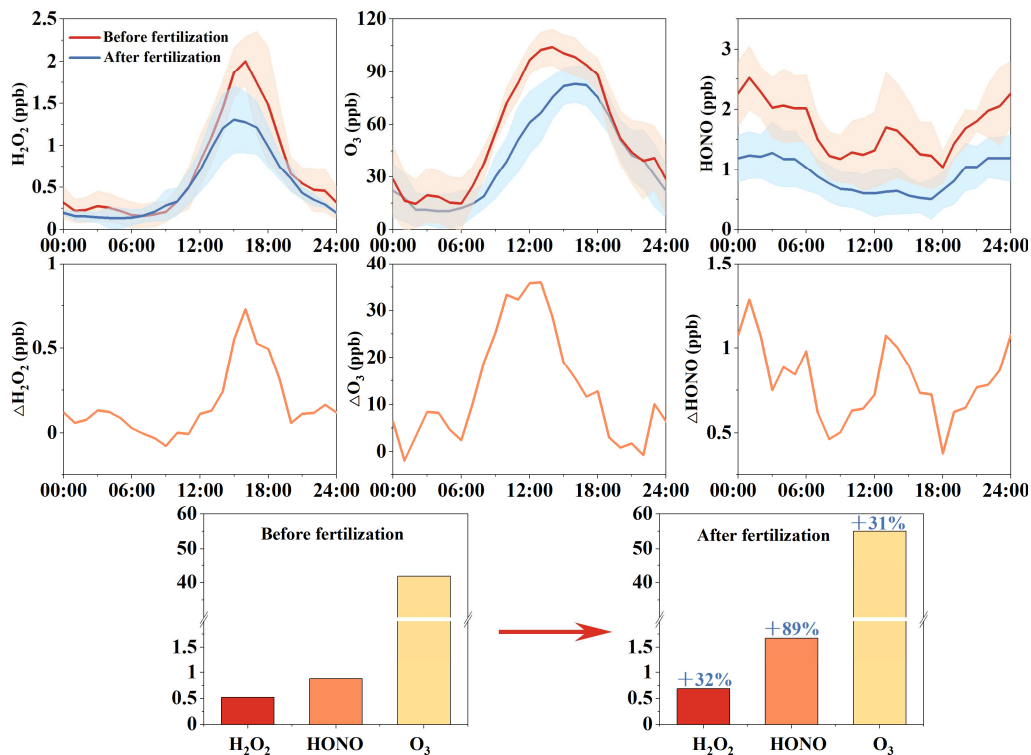
188 The summer campaign covered the important agricultural activities period like fertilization. The fertilization process
189 for the agricultural fields around our station was conducted on 13 June, 2017. Details about the fertilization event can
190 be found in our recent study, in which HONO emissions from the fertilized fields were discussed and its potential
191 impacts on O₃ and H₂O₂ were preliminarily mentioned (Xue et al., 2021). Figure 4 exhibited the time series of H₂O₂,
192 O₃ and solar radiation before (6-14 June) and after (14-21 June) the fertilization event. H₂O₂ and O₃ showed
193 pronounced diurnal patterns that were similar to those observed for solar radiation. After fertilization, both H₂O₂ and
194 O₃ diurnal peak values evidently increased (Figure 4 and Figure 5).



195

196 **Figure 4: Time series of H₂O₂, O₃ and solar radiation intensity before (6-14 June) and after (14-21 June) the**
197 **fertilization. The red line indicates the time when the fertilization event around the site began.**

198 To more accurately elaborate on the influence of fertilization events on H₂O₂, the H₂O₂ concentrations on 17 June,
199 which were mainly affected by biomass burning events as discussed in Section 3.1, were not taken into consideration.
200 The averaged concentrations of H₂O₂ and O₃ were a factor of 1.32 and 1.31 higher than the levels observed before the
201 fertilization events (Figure 5), but the solar radiation didn't show a significant change, indicating that fertilization may
202 promote the formation of H₂O₂ and O₃. Previous laboratory studies have reported that fertilized soil could be a source
203 of HONO with the use of nitrogen fertilizer (Su et al., 2011; Donaldson et al., 2014). Our previous work also provided
204 field evidence for soil HONO emission after fertilization at this site (Xue et al., 2019). Therefore, one can expect that
205 HONO concentrations may increase after the fertilization and subsequent HONO photolysis could release more OH
206 radicals compared to the period before fertilization, thereby accelerating the photochemical production of H₂O₂ and
207 O₃. Further analysis confirmed that after fertilization events the enhancements of H₂O₂ and O₃ were consistent with the
208 rising ambient HONO levels (Figure 5). Additionally, the significant increase in H₂O₂ (Δ H₂O₂) and O₃ (Δ O₃) appeared
209 around noontime, coincident with the HONO enhancement (Δ HONO) (Figure 5) and inferred soil HONO emission
210 flux in Xue et al. (2021). It is worth mentioning that Tan et al. (2017) reported high OH concentrations up to 3×10^7
211 cm⁻³ at the same rural site during a summer campaign in 2014, which was ascribed to local HONO emission from the
212 fertilized agricultural fields (Liu et al., 2019). Therefore, agricultural activities may strongly influence the atmospheric
213 oxidizing capacity and hence the concentrations of H₂O₂, which should be better constrained in atmospheric chemical
214 transport models to assess the impacts of H₂O₂ on regional air quality and global climate.

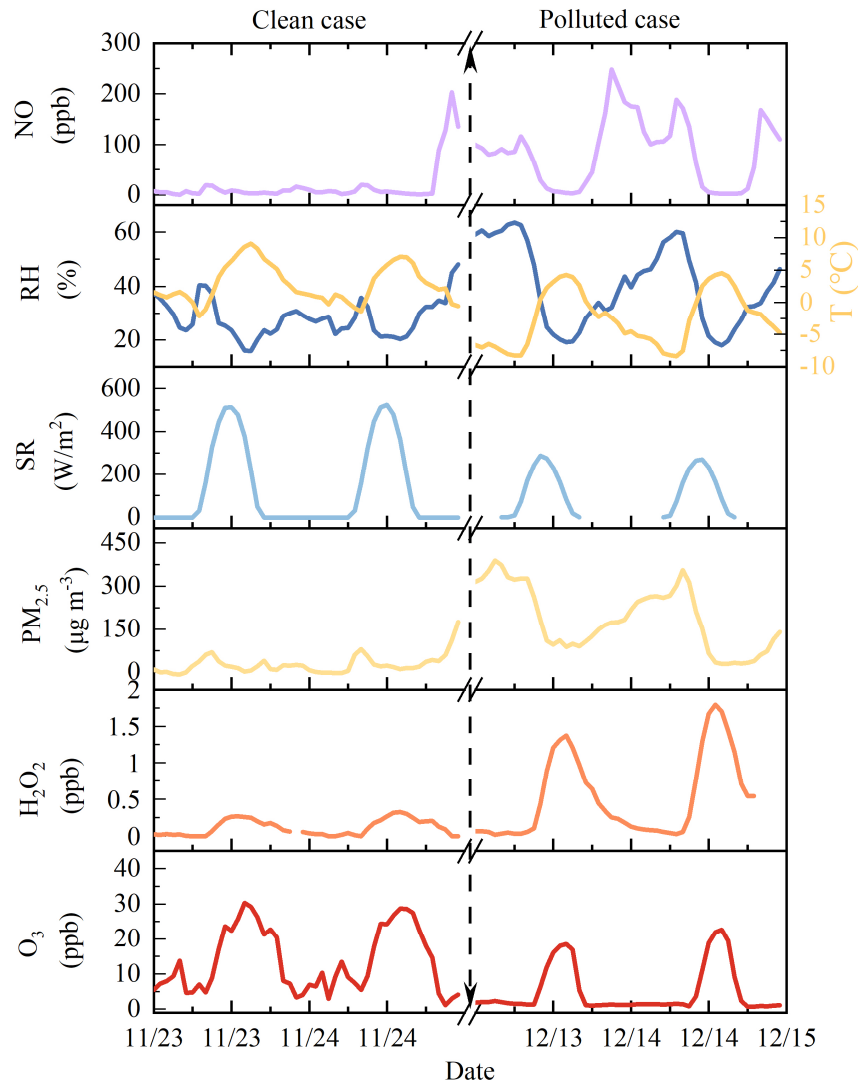


215

216 **Figure 5: Average concentrations of H₂O₂, HONO and O₃ before (6-14 June) and after (14-21 June) the**
 217 **fertilization in June 2017.**

218 **3.3 Influence of particles on H₂O₂ chemistry**

219 To investigate H₂O₂ production on clean and polluted days in the wintertime, representative cases were selected based
 220 on PM_{2.5} levels. Figure 6 shows H₂O₂ and other related chemical species and meteorological parameters measured
 221 during the winter campaign. In winter, the photochemical generation of OH radicals is weak as a consequence of
 222 significantly reduced solar radiation intensity, water vapor and ozone concentrations. Thus, the concentrations of
 223 secondary oxidants like H₂O₂ levels are typically believed to be low (Xue et al., 2016). On 23 and 24 November 2017
 224 during our field measurements (the clean case in Figure 6), the maximum solar radiation intensity was lower than 500
 225 W m⁻² and O₃ concentrations were less than 30 ppb, indicative of the low photochemical activity compared to summer
 226 seasons. The corresponding observed H₂O₂ concentrations were less than 0.35 ppb in the clean case.



227

228 **Figure 6:** H₂O₂, NO, PM_{2.5}, O₃, solar radiation intensity (Sa), relative humidity (RH) and temperature (T)
 229 measured in winter. Left panel: clean case (daily-averaged PM_{2.5} concentrations lower than 75 µg m⁻³) from 23
 230 to 25 November 2017; Right panel: polluted case (daily-averaged PM_{2.5} concentrations higher than 75 µg m⁻³)
 231 from 13 to 15 December 2018.

232 In contrast, during the polluted case, the maximum solar radiation intensity (~300 W m⁻²) and O₃ concentrations (~25
 233 ppb) were lower than that in the clean case, while the maximum H₂O₂ concentrations (> 1.5 ppb) in the polluted case

234 (Figure 6) were four times higher than that in the clean case. Contrary to our conventional thought, measured H₂O₂
 235 concentrations during the polluted periods were unexpectedly high, which were even similar to summer levels.
 236 It should be noted that the periods when H₂O₂ grew rapidly coincided with high NO levels exceeding several tens ppb
 237 (Figure 6). As discussed in the introduction section, the reaction rate of R2 was more than three orders of magnitude
 238 higher than R1 under the condition of 1 ppb NO. Therefore, gas-phase recombination of HO₂ radicals couldn't explain
 239 the high H₂O₂ levels observed. The peak value of H₂O₂ average diurnal pattern during polluted days (daily-averaged
 240 PM_{2.5}> 75 μg m⁻³) was evidently higher than that during clean days (daily-averaged PM_{2.5}< 75 μg m⁻³), indicating
 241 particles promoting H₂O₂ production (Figure S2). Moreover, H₂O₂ exhibited a pronounced diurnal pattern following
 242 the track of solar radiation, which implied that H₂O₂ was possibly photochemically produced. Taking all these hints
 243 into account, in-particle photochemical reactions are likely to produce the gas-phase H₂O₂. Some other typical cases
 244 (two clean and two polluted cases) were also identified and summarized in Table 1. These polluted cases with high
 245 H₂O₂ levels were observed in different years and should therefore be representative to reveal the promotion effect of
 246 particles on H₂O₂ production.

247 **Table 1. Summary of the clean and polluted cases**

Case type	Date	Average PM _{2.5} (μg m ⁻³)	H ₂ O ₂ maximum increase rate ^a (ppb h ⁻¹)	Maximum H ₂ O ₂ (ppb)
Clean	8 December 2017	14	0.05	0.36
	4 December 2018	32	0.04	0.21
Polluted	21 December 2017	135	0.266	1.16
	22 December 2017	216	0.267	1.19

248 ^aH₂O₂ increase rate was calculated as (C_{t+1}-C_t)/1 h. C_t represents the hourly-averaged H₂O₂ concentrations at time t.

249

250 Previous studies have reported the photochemical production of H₂O₂ free of NO suppression effect in the atmospheric
 251 aqueous phase like in clouds and fog water (Faust et al., 1993; Anastasio et al., 1994; Zuo and Hoigné, 1993;
 252 Anastasio et al., 1997). The observation is also consistent to our recent chamber and flow tube studies which revealed

253 that photochemical aging of particles involving organic chromophores could produce gas-phase H₂O₂ (Ye et al., 2021;
254 Liu et al., 2021). Organic chromophores have long been identified as important contributors to the aqueous photo-
255 production of H₂O₂ (Faust et al., 1993; Anastasio et al., 1997; Arellanes et al., 2006; Fang et al., 2019). The filter
256 sample analysis showed that particles at our sampling site in winter contained a significant concentration of light-
257 absorbing chromophores (Wang et al., 2020). Considering the photoactivity and abundance of organic chromophores
258 in particles (Poschl and Shiraiwa, 2015; Herrmann et al., 2015), particles may have a crucial effect on the
259 photochemical production of gas-phase H₂O₂. In winter, especially under the conditions of high NO presence, this
260 multiphase reaction channel for H₂O₂ formation, which is less sensitive to NO concentration, may play a more
261 important role than the classical self-reaction of HO₂ radicals, thereby contributing to more sulfate formation. The
262 enhanced photochemical release of H₂O₂ and subsequent oxidation of SO₂ could also shed light on the discrepancy
263 between observed and modeled sulfate concentrations during polluted periods.

264 A recent study found evident O₂⁻ and sulfate production on Beijing urban PM_{2.5} filter samples under simulated UV
265 radiation (Zhang et al., 2020). This study also indicated that H₂O₂ might be produced in the aging process of PM_{2.5} and
266 subsequent H₂O₂-oxidation leads to the formation of sulfate, which is in agreement with our findings based on field
267 measurements. Further work is needed to fully understand this unique H₂O₂-production pathway and assess its impacts
268 on the global H₂O₂ abundance and sulfate budget.

269 **4 Conclusions and implications**

270 Several field campaigns with measurements on atmospheric H₂O₂ and related parameters were conducted in the rural
271 NCP during different seasons. It allows a determination of special factors (biomass burning, fertilization, and ambient
272 particles) influencing gas-phase H₂O₂ concentrations in this region. First, biomass burning plumes with high H₂O₂
273 concentrations up to 9 ppb were observed during a summer campaign. The measured H₂O₂ rapidly increased from 1
274 ppb to 9 ppb in two hours. Such a high H₂O₂ level and rapid increase can't be solely explained by photochemical
275 production. Along with the analysis of back-trajectory and fire spots data, high H₂O₂ level was mainly attributed to

276 primary emission by large areas of biomass burning event. Second, a significant H₂O₂ increase was observed after the
277 agricultural nitrogen fertilization event in the summer. We found concurrent elevation of HONO levels compared to
278 that before the fertilization events. The enhanced HONO levels, caused by the soil HONO emission from the fertilized
279 agricultural fields, promoted the atmospheric oxidizing capacity and accelerated the production of secondary oxidants
280 like H₂O₂ and O₃. Third, high H₂O₂ concentrations exceeding 1.5 ppb, were observed under the presence of several
281 tens ppb NO during pollution episodes in the winter campaigns. Under such high NO conditions, the traditional gas-
282 phase channel for H₂O₂ formation would be greatly suppressed so that it was far to explained the measured H₂O₂. High
283 H₂O₂ cases were typically accompanied by high PM_{2.5} levels, suggesting the potential role of particles in H₂O₂
284 production. Analogous to the aqueous H₂O₂ production in the atmospheric aqueous phase like clouds by organic
285 chromophores, high H₂O₂ during winter polluted periods might be produced by chromophores in the particle phase
286 considering the prevalence of chromophores in particles at this site.

287 Very limited measurements on atmospheric H₂O₂ in China, especially in polluted regions, are currently available
288 despite its important role in the atmospheric oxidizing capacity and sulfate aerosol formation. This study provides a
289 unique dataset (one summer and two winter campaigns) of H₂O₂ measurements in the NCP, which will benefit the
290 assessment of model performance in the prediction of H₂O₂ concentrations and its potential regional and global
291 impacts. Our results also highlight the important roles of the special factors (biomass burning, fertilization, and
292 ambient particles) in enhancing the concentrations of gas-phase H₂O₂. The enhanced H₂O₂ production influenced by
293 these special factors will contribute to the oxidizing capacity of the atmosphere and hence more sulfate aerosol
294 formation, which has a crucial effect on air quality and direct forcing of the earth's climate. Additionally, particle-
295 bound H₂O₂ will further produce OH radical by photolysis and Fenton reaction, which will contribute to the aerosol
296 aging and oxidizing organics within particles. Furthermore, reactive oxygen species (e.g., H₂O₂, OH, O₂⁻) are at least
297 partly responsible for the particle-related adverse health effect. The in-particle production of H₂O₂ may constitute a
298 public risk to human health. However, these special factors influencing H₂O₂ concentrations are not well considered in
299 model estimates of H₂O₂ and may limit the accurate prediction of the H₂O₂ budget in the atmosphere and its associated

300 climate and health effects. Hence, further research on the factors in controlling H₂O₂ concentrations and model
301 improvements in H₂O₂ simulations are greatly warranted.

302

303 *Data availability.* Observation data are available at <https://zenodo.org/record/4456345#.YAp7DzMufX8>

304 *Competing interests.* The authors declare that they have no conflict of interest.

305 *Acknowledgements.* This work was supported by the National Natural Science Foundation of China (Nos. 41727805,
306 41975164, 91544211, 22076202, 21976190, 41905109, 21876186), the China Postdoctoral Foundation
307 (No.2021M700214), the PIVOTS project provided by the Region Centre -Val de Loire (ARD 2020 program and CPER
308 2015 - 2020), and the Labex VOLTAIRE project (ANR-10-LABX-100-01). The authors thank Miss Wuqi Shen for the
309 help with Graphical Abstract plotting.

310 **5 References**

311 Allen, H. M., Crouse, J. D., Kim, M. J., Teng, A. P., Ray, E. A., McKain, K., Sweeney, C., and Wennberg, P. O.: H₂O₂
312 and CH₃OOH (MHP) in the Remote Atmosphere: 1. Global Distribution and Regional Influences, *Journal of Geophysical*
313 *Research: Atmospheres*, 127, e2021JD035701, <https://doi.org/10.1029/2021JD035701>, 2022.

314 Anastasio, C., Faust, B. C., and Allen, J. M.: Aqueous phase photochemical formation of hydrogen peroxide in authentic
315 cloud waters, *Journal of Geophysical Research: Atmospheres*, 99, 8231-8248, 1994.

316 Anastasio, C., Faust, B. C., and Rao, C. J.: Aromatic carbonyl compounds as aqueous-phase photochemical sources of
317 hydrogen peroxide in acidic sulfate aerosols, fogs, and clouds .1. Non-phenolic methoxybenzaldehydes and
318 methoxyacetophenones with reductants (phenols), *Environ Sci Technol*, 31, 218-232, 1997.

319 Andreae, M. O.: Emission of trace gases and aerosols from biomass burning - an updated assessment, *Atmos Chem Phys*, 19,
320 8523-8546, 2019.

321 Arellanes, C., Paulson, S. E., Fine, P. M., and Sioutas, C.: Exceeding of Henry's law by hydrogen peroxide associated with
322 urban aerosols, *Environ Sci Technol*, 40, 4859-4866, 2006.

323 Atkinson, R., Baulch, D. L., Cox, R. A., Crowley, J. N., Hampson, R. F., Hynes, R. G., Jenkin, M. E., Rossi, M. J., and Troe,
324 J.: Evaluated kinetic and photochemical data for atmospheric chemistry: Volume I - gas phase reactions of O-x, HOx,
325 NOx and SOx species, *Atmos Chem Phys*, 4, 1461-1738, 2004.

326 Becker, K. H., Brockmann, K. J., and Bechara, J.: Production of hydrogen peroxide in forest air by reaction of ozone with
327 terpenes, *Nature*, 346, 256-258, 1990.

328 Calvert, J. G., and Stockwell, W. R.: Acid generation in the troposphere by gas-phase chemistry, *Environ Sci Technol*, 17,
329 428A-443A, 1983.

330 Crowley, J. N., Pouvesle, N., Phillips, G. J., Axinte, R., Fischer, H., Petäjä, T., Nölscher, A., Williams, J., Hens, K., and
331 Harder, H.: Insights into HOx and ROx chemistry in the boreal forest via measurement of peroxyacetic acid, peroxyacetic
332 nitric anhydride (PAN) and hydrogen peroxide, *Atmos Chem Phys*, 2018.

333 Das, M., and Aneja, V. P.: Analysis of Gaseous-Hydrogen Peroxide Concentrations in Raleigh, North-Carolina, *J Air Waste*
334 *Manage*, 44, 176-180, 1994.

335 Donaldson, M. A., Bish, D. L., and Raff, J. D.: Soil surface acidity plays a determining role in the atmospheric-terrestrial
336 exchange of nitrous acid, *P Natl Acad Sci USA*, 111, 18472-18477, 2014.

337 Elshorbany, Y. F., Kleffmann, J., Kurtenbach, R., Lissi, E., Rubio, M., Villena, G., Gramsch, E., Rickard, A. R., Pilling, M.
338 J., and Wiesen, P.: Seasonal dependence of the oxidation capacity of the city of Santiago de Chile, *Atmos Environ*, 44,
339 5383-5394, 2010.

340 Fang, T., Lakey, P. S. J., Weber, R. J., and Shiraiwa, M.: Oxidative Potential of Particulate Matter and Generation of
341 Reactive Oxygen Species in Epithelial Lining Fluid, *Environ Sci Technol*, 53, 12784-12792, 2019.

342 Faust, B. C., Anastasio, C., Allen, J. M., and Arakaki, T.: Aqueous-phase photochemical formation of peroxides in authentic
343 cloud and fog waters, *Science*, 260, 73-75, 1993.

344 Fischer, H., Axinte, R., Bozem, H., Crowley, J. N., Ernest, C., Gilge, S., Hafermann, S., Harder, H., Hens, K., and Janssen,
345 R. H.: Diurnal variability, photochemical production and loss processes of hydrogen peroxide in the boundary layer over
346 Europe, *Atmos Chem Phys*, 19, 11953-11968, 2019.

347 Fuzzi, S., Baltensperger, U., Carslaw, K., Decesari, S., van Der Gon, H. D., Facchini, M. C., Fowler, D., Koren, I., Langford,
348 B., Lohmann, U., Nemitz, E., Pandis, S., Riipinen, I., Rudich, Y., Schaap, M., Slowik, J. G., Spracklen, D. V., Vignati, E.,
349 Wild, M., Williams, M., and Gilardoni, S.: Particulate matter, air quality and climate: lessons learned and future needs,
350 *Atmos Chem Phys*, 15, 8217-8299, 10.5194/acp-15-8217-2015, 2015.

351 Grantz, D. A., Garner, J. H. B., and Johnson, D. W.: Ecological effects of particulate matter, *Environ Int*, 29, 213-239, 2003.

352 Guo, J., Tilgner, A., Yeung, C., Wang, Z., Louie, P. K. K., Luk, C. W. Y., Xu, Z., Yuan, C., Gao, Y., Poon, S., Herrmann,
353 H., Lee, S., Lam, K. S., and Wang, T.: Atmospheric Peroxides in a Polluted Subtropical Environment: Seasonal Variation,
354 Sources and Sinks, and Importance of Heterogeneous Processes, *Environ Sci Technol*, 48, 1443-1450,
355 10.1021/es403229x, 2014.

356 Hamilton Jr, E. J., and Lii, R. R.: The Dependence on H₂O and on NH₃ of the Kinetics of the self-reaction of HO₂ in the
357 gas-phase formation of HO₂· H₂O and HO₂· NH₃ complexes, *International Journal of Chemical Kinetics*, 9, 875-885,
358 1977.

359 He, S. Z., Chen, Z. M., Zhang, X., Zhao, Y., Huang, D. M., Zhao, J. N., Zhu, T., Hu, M., and Zeng, L. M.: Measurement of
360 atmospheric hydrogen peroxide and organic peroxides in Beijing before and during the 2008 Olympic Games: Chemical
361 and physical factors influencing their concentrations, *J Geophys Res-Atmos*, 115, Artn D1730710.1029/2009jd013544,
362 2010.

363 Heland, J., Kleffmann, J., Kurtenbach, R., and Wiesen, P.: A new instrument to measure gaseous nitrous acid (HONO) in the
364 atmosphere, *Environ. Sci. Technol.*, 35, 3207–3212, <https://doi.org/10.1021/es000303t>, 2001

365 Herrmann, H., Schaefer, T., Tilgner, A., Styler, S. A., Weller, C., Teich, M., and Otto, T.: Tropospheric Aqueous-Phase
366 Chemistry: Kinetics, Mechanisms, and Its Coupling to a Changing Gas Phase, *Chem Rev*, 115, 4259-4334, 2015.

367 Hoffmann, M., and Edwards, J.: Kinetics of the oxidation of sulfite by hydrogen peroxide in acidic solution, *The Journal of*
368 *Physical Chemistry*, 79, 2096-2098, 1975.

369 Hua, W., Chen, Z. M., Jie, C. Y., Kondo, Y., Hofzumahaus, A., Takegawa, N., Chang, C. C., Lu, K. D., Miyazaki, Y., Kita,
370 K., Wang, H. L., Zhang, Y. H., and Hu, M.: Atmospheric hydrogen peroxide and organic hydroperoxides during PRIDE-

371 PRD'06, China: their concentration, formation mechanism and contribution to secondary aerosols, *Atmos Chem Phys*, 8,
372 6755-6773, DOI 10.5194/acp-8-6755-2008, 2008.

373 Kleinman, L. I.: Photochemical formation of peroxides in the boundary layer, *Journal of Geophysical Research:*
374 *Atmospheres*, 91, 10889-10904, 1986.

375 Lee, M., Heikes, B. G., Jacob, D. J., Sachse, G., and Anderson, B.: Hydrogen peroxide, organic hydroperoxide, and
376 formaldehyde as primary pollutants from biomass burning, *Journal of Geophysical Research: Atmospheres*, 102, 1301-
377 1309, 10.1029/96jd01709, 1997.

378 Lee, M., Kie, J. A., Kim, Y. M., and Lee, G.: Characteristics of atmospheric hydrogen peroxide variations in Seoul megacity
379 during 2002-2004, *Sci Total Environ*, 393, 299-308, 10.1016/j.scitotenv.2007.11.037, 2008.

380 Lee, M. H., Heikes, B. G., and O'Sullivan, D. W.: Hydrogen peroxide and organic hydroperoxide in the troposphere: A
381 review, *Atmos Environ*, 34, 3475-3494, Doi 10.1016/S1352-2310(99)00432-X, 2000.

382 Liang, H., Chen, Z. M., Huang, D., Zhao, Y., and Li, Z. Y.: Impacts of aerosols on the chemistry of atmospheric trace gases:
383 a case study of peroxides and HO₂ radicals, *Atmos Chem Phys*, 13, 11259-11276, 10.5194/acp-13-11259-2013, 2013.

384 Liu, M. X., Song, Y., Yao, H., Kang, Y. N., Li, M. M., Huang, X., and Hu, M.: Estimating emissions from agricultural fires
385 in the North China Plain based on MODIS fire radiative power, *Atmos Environ*, 112, 326-334, 2015.

386 Liu, P. F., Zhang, C. L., Xue, C. Y., Mu, Y. J., Liu, J. F., Zhang, Y. Y., Tian, D., Ye, C., Zhang, H. X., and Guan, J.: The
387 contribution of residential coal combustion to atmospheric PM_{2.5} in northern China during winter, *Atmos Chem Phys*, 17,
388 11503-11520, 10.5194/acp-17-11503-2017, 2017.

389 Liu, P., Ye, C., Zhang, C., He, G., Xue, C., Liu, J., Liu, C., Zhang, Y., Song, Y., Li, X., Wang, X., Chen, J., He, H.,
390 Herrmann, H., and Mu, Y.: Photochemical Aging of Atmospheric Fine Particles as a Potential Source for Gas-Phase
391 Hydrogen Peroxide, *Environ Sci Technol*, 10.1021/acs.est.1c04453, 2021.

392 Liu, Y., Lu, K., Li, X., Dong, H., Tan, Z., Wang, H., Zou, Q., Wu, Y., Zeng, L., Hu, M., Min, K.-E., Kecorius, S.,
393 Wiedensohler, A., and Zhang, Y.: A Comprehensive Model Test of the HONO Sources Constrained to Field
394 Measurements at Rural North China Plain, *Environ Sci Technol*, 53, 3517-3525, 10.1021/acs.est.8b06367, 2019.

395 Ma, X. F., Tan, Z. F., Lu, K. D., Yang, X. P., Liu, Y. H., Li, S. L., Li, X., Chen, S. Y., Novelli, A., Cho, C. M., Zeng, L. M.,
396 Wahner, A., and Zhang, Y. H.: Winter photochemistry in Beijing: Observation and model simulation of OH and HO₂
397 radicals at an urban site, *Sci Total Environ*, 685, 85-95, 2019.

398 Nel, A.: Air pollution-related illness: Effects of particles, *Science*, 308, 804-806, 10.1126/science.1108752, 2005.

399 Nunnermacker, L. J., Weinstein-Lloyd, J. B., Hillery, B., Giebel, B., Kleinman, L. I., Springston, S. R., Daum, P. H.,
400 Gaffney, J., Marley, N., and Huey, G.: Aircraft and ground-based measurements of hydroperoxides during the 2006
401 MILAGRO field campaign, *Atmos Chem Phys*, 8, 7619-7636, 10.5194/acp-8-7619-2008, 2008.

402 Penkett, S. A., Jones, B. M. R., Brice, K. A., and Eggleton, A. E. J.: Importance of Atmospheric Ozone and Hydrogen-
403 Peroxide in Oxidizing Sulfur-Dioxide in Cloud and Rainwater, *Atmos Environ*, 13, 123-137, Doi 10.1016/0004-
404 6981(79)90251-8, 1979.

405 Poschl, U., and Shiraiwa, M.: Multiphase Chemistry at the Atmosphere-Biosphere Interface Influencing Climate and Public
406 Health in the Anthropocene, *Chem Rev*, 115, 4440-4475, 2015.

407 Qin, M., Chen, Z., Shen, H., Li, H., Wu, H., and Wang, Y.: Impacts of heterogeneous reactions to atmospheric peroxides:
408 Observations and budget analysis study, *Atmos Environ*, 183, 144-153, 10.1016/j.atmosenv.2018.04.005, 2018.

409 Reeves, C. E., and Penkett, S. A.: Measurements of peroxides and what they tell us, *Chem Rev*, 103, 5199-5218,
410 10.1021/cr0205053, 2003.

411 Sillman, S.: The use of NO_y, H₂O₂, and HNO₃ as indicators for ozone-NO_x-hydrocarbon sensitivity in urban locations,
412 *Journal of Geophysical Research: Atmospheres*, 100, 14175-14188, 1995.

413 Sillman, S., He, D., Pippin, M. R., Daum, P. H., Imre, D. G., Kleinman, L. I., Lee, J. H., and Weinstein-Lloyd, J.: Model
414 correlations for ozone, reactive nitrogen, and peroxides for Nashville in comparison with measurements: Implications for
415 O₃-NO_x-hydrocarbon chemistry, *Journal of Geophysical Research: Atmospheres*, 103, 22629-22644, 1998.

416 Slater, E. J., Whalley, L. K., Woodward-Massey, R., Ye, C. X., Lee, J. D., Squires, F., Hopkins, J. R., Dunmore, R. E.,
417 Shaw, M., Hamilton, J. F., Lewis, A. C., Crilley, L. R., Kramer, L., Bloss, W., Vu, T., Sun, Y. L., Xu, W. Q., Yue, S. Y.,
418 Ren, L. J., Acton, W. J. F., Hewitt, C. N., Wang, X. M., Fu, P. Q., and Heard, D. E.: Elevated levels of OH observed in

419 haze events during wintertime in central Beijing, *Atmos Chem Phys*, 20, 14847-14871, 10.5194/acp-20-14847-2020,
420 2020.

421 Stockwell, W. R., Kirchner, F., Kuhn, M., and Seefeld, S.: A new mechanism for regional atmospheric chemistry modeling,
422 *J Geophys Res-Atmos*, 102, 25847-25879, 1997.

423 Su, H., Cheng, Y. F., Oswald, R., Behrendt, T., Trebs, I., Meixner, F. X., Andreae, M. O., Cheng, P., Zhang, Y., and Poschl,
424 U.: Soil Nitrite as a Source of Atmospheric HONO and OH Radicals, *Science*, 333, 1616-1618, 2011.

425 Tan, Z. F., Fuchs, H., Lu, K. D., Hofzumahaus, A., Bohn, B., Broch, S., Dong, H. B., Gomm, S., Haseler, R., He, L. Y.,
426 Holland, F., Li, X., Liu, Y., Lu, S. H., Rohrer, F., Shao, M., Wang, B. L., Wang, M., Wu, Y. S., Zeng, L. M., Zhang, Y. S.,
427 Wahner, A., and Zhang, Y. H.: Radical chemistry at a rural site (Wangdu) in the North China Plain: observation and
428 model calculations of OH, HO₂ and RO₂ radicals, *Atmos Chem Phys*, 17, 663-690, 10.5194/acp-17-663-2017, 2017.

429 Tan, Z., Lu, K., Jiang, M., Su, R., Dong, H., Zeng, L., Xie, S., Tan, Q., and Zhang, Y.: Exploring ozone pollution in
430 Chengdu, southwestern China: A case study from radical chemistry to O₃-VOC-NO_x sensitivity, *Sci Total Environ*, 636,
431 775-786, <https://doi.org/10.1016/j.scitotenv.2018.04.286>, 2018.

432 Vermeuel, M. P., Novak, G. A., Alwe, H. D., Hughes, D. D., Kaleel, R., Dickens, A. F., Kenski, D., Czarnetzki, A. C.,
433 Stone, E. A., and Stanier, C. O.: Sensitivity of Ozone Production to NO_x and VOC Along the Lake Michigan Coastline,
434 *Journal of Geophysical Research: Atmospheres*, 124, 10989-11006, 2019.

435 Walker, S. J., Evans, M. J., Jackson, A. V., Steinbacher, M., Zellweger, C., and McQuaid, J. B.: Processes controlling the
436 concentration of hydroperoxides at Jungfraujoch Observatory, Switzerland, *Atmos Chem Phys*, 6, 5525-5536, DOI
437 10.5194/acp-6-5525-2006, 2006.

438 Wang, X., Gemayel, R., Hayeck, N., Perrier, S., Charbonnel, N., Xu, C., Chen, H., Zhu, C., Zhang, L., and Wang, L.:
439 Atmospheric photosensitization: a new pathway for sulfate formation, *Environ Sci Technol*, 2020.

440 Wang, Y., Chen, Z. M., Wu, Q. Q., Liang, H., Huang, L. B., Li, H., Lu, K. D., Wu, Y. S., Dong, H. B., Zeng, L. M., and
441 Zhang, Y. H.: Observation of atmospheric peroxides during Wangdu Campaign 2014 at a rural site in the North China
442 Plain, *Atmos Chem Phys*, 16, 10985-11000, 10.5194/acp-16-10985-2016, 2016.

443 Wang, Y. X., Zhang, Q. Q., Jiang, J. K., Zhou, W., Wang, B. Y., He, K. B., Duan, F. K., Zhang, Q., Philip, S., and Xie, Y.
444 Y.: Enhanced sulfate formation during China's severe winter haze episode in January 2013 missing from current models, *J*
445 *Geophys Res-Atmos*, 119, 2014.

446 Watanabe, K., Yachi, C., Nishibe, M., Michigami, S., Saito, Y., Eda, N., Yamazaki, N., and Hirai, T.: Measurements of
447 atmospheric hydroperoxides over a rural site in central Japan during summers using a helicopter, *Atmos Environ*, 146,
448 174-182, 10.1016/j.atmosenv.2016.06.074, 2016.

449 Watanabe, K., Yachi, C., Song, X. J., Kakuyama, S., Nishibe, M., and Michigami, S.: Measurements of atmospheric
450 hydroperoxides at a rural site in central Japan, *J Atmos Chem*, 75, 71-84, 2018.

451 Watson, J. G., Chow, J. C., and Houck, J. E.: PM_{2.5} chemical source profiles for vehicle exhaust, vegetative burning,
452 geological material, and coal burning in Northwestern Colorado during 1995, *Chemosphere*, 43, 1141-1151, 2001.

453 Wiedinmyer, C., Akagi, S. K., Yokelson, R. J., Emmons, L. K., Al-Saadi, J. A., Orlando, J. J., and Soja, A. J.: The Fire
454 INventory from NCAR (FINN): a high resolution global model to estimate the emissions from open burning, *Geosci.*
455 *Model Dev.*, 4, 625-641, 10.5194/gmd-4-625-2011, 2011.

456 Xue, C., Ye, C., Zhang, Y., Ma, Z., Liu, P., Zhang, C., Zhao, X., Liu, J., and Mu, Y.: Development and application of a twin
457 open-top chambers method to measure soil HONO emission in the North China Plain, *Sci Total Environ*, 659, 621-631,
458 2019.

459 Xue, C., Ye, C., Zhang, C., Catoire, V., Liu, P., Gu, R., Zhang, J., Ma, Z., Zhao, X., Zhang, W., Ren, Y., Krysztofiak, G.,
460 Tong, S., Xue, L., An, J., Ge, M., Mellouki, A., and Mu, Y.: Evidence for Strong HONO Emission from Fertilized
461 Agricultural Fields and its Remarkable Impact on Regional O₃ Pollution in the Summer North China Plain, *ACS Earth*
462 *and Space Chemistry*, 10.1021/acsearthspacechem.0c00314, 2021.

463 Xue, C. Y., Zhang, C. L., Ye, C., Liu, P. F., Catoire, V., Krysztofiak, G., Chen, H., Ren, Y. G., Zhao, X. X., Wang, J. H.,
464 Zhang, F., Zhang, C. X., Zhang, J. W., An, J. L., Wang, T., Chen, J. M., Kleffmann, J., Mellouki, A., and Mu, Y. J.:
465 HONO Budget and Its Role in Nitrate Formation in the Rural North China Plain, *Environ Sci Technol*, 54, 11048-11057,
466 2020.

467 Xue, J., Yuan, Z. B., Griffith, S. M., Yu, X., Lau, A. K. H., and Yu, J. Z.: Sulfate Formation Enhanced by a Cocktail of High
468 NO_x, SO₂, Particulate Matter, and Droplet pH during Haze-Fog Events in Megacities in China: An Observation-Based
469 Modeling Investigation, *Environ Sci Technol*, 50, 7325-7334, 2016.

470 Ye, C., Liu, P., Ma, Z., Xue, C., Zhang, C., Zhang, Y., Liu, J., Liu, C., Sun, X., and Mu, Y.: High H₂O₂ Concentrations
471 Observed during Haze Periods during the Winter in Beijing: Importance of H₂O₂ Oxidation in Sulfate Formation,
472 *Environmental Science & Technology Letters*, 10.1021/acs.estlett.8b00579, 2018.

473 Ye, C., Chen, H., Hoffmann, E. H., Mettke, P., Tilgner, A., He, L., Mutzel, A., Brüggemann, M., Poulain, L., and Schaefer,
474 T.: Particle-Phase Photoreactions of HULIS and TMIs Establish a Strong Source of H₂O₂ and Particulate Sulfate in the
475 Winter North China Plain, *Environ Sci Technol*, 2021.

476 Yokelson, R. J., Crouse, J. D., DeCarlo, P. F., Karl, T., Urbanski, S., Atlas, E., Campos, T., Shinozuka, Y., Kapustin, V.,
477 Clarke, A. D., Weinheimer, A., Knapp, D. J., Montzka, D. D., Holloway, J., Weibring, P., Flocke, F., Zheng, W., Toohey,
478 D., Wennberg, P. O., Wiedinmyer, C., Mauldin, L., Fried, A., Richter, D., Walega, J., Jimenez, J. L., Adachi, K., Buseck,
479 P. R., Hall, S. R., and Shetter, R.: Emissions from biomass burning in the Yucatan, *Atmos. Chem. Phys.*, 9, 5785-5812,
480 10.5194/acp-9-5785-2009, 2009.

481 Yu, D., Tan, Z., Lu, K., Ma, X., Li, X., Chen, S., Zhu, B., Lin, L., Li, Y., Qiu, P., Yang, X., Liu, Y., Wang, H., He, L.,
482 Huang, X., and Zhang, Y.: An explicit study of local ozone budget and NO_x-VOCs sensitivity in Shenzhen China, *Atmos*
483 *Environ*, 224, 117304, <https://doi.org/10.1016/j.atmosenv.2020.117304>, 2020.

484 Zhang, Q., Liu, J., He, Y., Yang, J., Gao, J., Liu, H., Tang, W., Chen, Y., Fan, W., and Chen, X.: Measurement of hydrogen
485 peroxide and organic hydroperoxide concentrations during autumn in Beijing, China, *J Environ Sci-China*, 64, 72-81,
486 2018.

487 Zhang, Y., Bao, F., Li, M., Xia, H., Huang, D., Chen, C., and Zhao, J.: Photoinduced Uptake and Oxidation of SO₂ on
488 Beijing Urban PM_{2.5}, *Environ Sci Technol*, 10.1021/acs.est.0c01532, 2020.

489 Zheng, B., Zhang, Q., Zhang, Y., He, K. B., Wang, K., Zheng, G. J., Duan, F. K., Ma, Y. L., and Kimoto, T.: Heterogeneous
490 chemistry: a mechanism missing in current models to explain secondary inorganic aerosol formation during the January
491 2013 haze episode in North China, *Atmos Chem Phys*, 15, 2031-2049, 10.5194/acp-15-2031-2015, 2015.

492 Zuo, Y., and Hoigné, J.: Evidence for photochemical formation of H₂O₂ and oxidation of SO₂ in authentic fog water,
493 Science, 260, 71-73, 1993.